Control of a Two-Phase Linear Stepping Motor with Three-Phase Voltage Source Inverter

Sheng-Ming Yang, Feng-Chieh Lin, and Ming-Chung Chen
Department of Mechanical and Electro-mechanical Engineering
Tamkang University, Tamsui
Taipei County, Taiwan 25137

Abstract - **This paper presents a current control scheme for the micro-stepping of two-phase linear stepping motor drive using three-phase voltage source inverter. The purpose of this scheme is for cost reduction since all the control loops are executed digitally and standard three-phase voltage source inverter is used. Because the operating frequency is quite high, the cross-coupling between motor phase currents are removed to preserve the dynamical characteristics of the current controller as frequency varies. A space vector PWM for two-phase motor is also presented. The scheme is based on the principle of harmonic injection for three-phase motors. Because the inverter leg voltages are imbalanced when driving a two-phase motor, the dead-time effect of the inverter power switches must be compensated for or significant current error may occur. Good static and dynamic performances were obtained in the experimental verifications.**

Keywords: linear stepping motor, micro-stepping, current control, space vector PWM

I. INTRODUCTION

Because of its high positional accuracy and simplicity in mechanical linkage, linear hybrid stepping motor (LSM) has gained widespread applications in factory automations. Hybrid stepping motors are synchronous motors with high number of pole pairs. Majority of them are two-phase and operated in open positional loop with micro-stepping, where motor currents are controlled in sinusoidal fashion to increase positioning accuracy and to reduce rotor resonant oscillations. Typically, phase currents in a LSM are controlled independently to each other, and each phase has an analog current loop with an H-bridge to modulate motor voltage for the desire current [1]. As a feedback is not required micro-stepped LSM presents a cost advantage in comparison to PM synchronous motor drives. Consequently, LSM drives are often used in cost sensitive products.

Owing to the advancements of modern microprocessor technologies, cost reduction on LSM drives can be achieved through: 1) perform all the control actions digitally to simplify circuit design, 2) standardization of hardware to reduce cost. Many modern microprocessors are designed specifically for all-digital control of three-phase motors such as induction or synchronous motors, and rarely for micro-stepped stepping motors. Therefore, significant costs can be saved if these microprocessors and standard voltage source inverter (VSI) circuits can be used to drive LSMs. In order to achieve this objective, the motor drive requires a PWM strategy that can drive two-phase motor with three-phase VSI, and the control loops can be implemented simply in microprocessors and has comparable or better performance compared to their analog counterparts.

When driven with three-phase inverter, the windings of a two-phase LSM are generally connected in series, and the two open ends and the common point are connected to the three inverter legs [2]. Because the circuits seen by inverter legs are not balanced, the space vectors of the switching states form an asymmetric hexagonal [3]. Consequently, PWM schemes for three-phase motors cannot be applied directly. A number of PWM strategies for the control of this unbalanced circuit structure have been proposed previously [2-4]. But the frequency ranges considered in these reports were limited to the operating range of typical induction motors. For LSMs, the operating frequency is much higher than induction motors due to their high pole-pair numbers. Another attribute associated with this unbalanced circuit structure is that motor currents are very sensitive to the inverter voltage errors. For example, significant magnitude and phase errors occurred in motor currents if dead-time of the inverter power switches are not properly compensated for. This also implies that steady state error in the current controller should be minimized to avoid imbalanced motor phase currents.

In this paper, a control scheme which consisting of a synchronous frame current regulator and a space vector PWM voltage modulator is proposed for the micro-stepping of two-phase linear stepping motors. The current controller does not have steady state error when the motor is running at constant speed. The PWM strategy is based on the principle of harmonic injection for three-phase motors. A dead-time compensation scheme suitable for micro-stepping control is also presented to minimize voltage error at the inverter outputs.

II. MOTOR MODEL

The model of a two-phase linear hybrid stepping motor can be expressed in a frame rotating synchronously with the excitation current as [5],

$$\begin{bmatrix} V_{qe} \\ V_{de} \end{bmatrix} = \begin{bmatrix} r + L\cdot s & L\omega_e \\ -L\omega_e & r + L\cdot s \end{bmatrix} \begin{bmatrix} i_{qe} \\ i_{de} \end{bmatrix} + k_m \left(\frac{2\pi}{p_t}\right) v \begin{bmatrix} \cos(\Delta\theta_e) \\ \sin(\Delta\theta_e) \end{bmatrix} \quad (1)$$

0-7803-7817-2/03/$17.00 ©2003 IEEE

where V_{qe}, V_{de}, i_{qe} and i_{de} are qd-axis voltages and currents, respectively, ω_e is the excitation frequency, $\Delta\theta_e$ is the angle between current vector and rotor electrical position, i.e. $\Delta\theta_e = \theta_e - \frac{2\pi}{p_t}x$, p_t is the pole pitch, x and v are the rotor position and velocity, respectively, and r, L, and k_m are motor parameters. The motor generated force is

$$F_e = k_t\left[\cos(\Delta\theta_e) \quad \sin(\Delta\theta_e)\right]\begin{bmatrix} i_{qe} \\ i_{de} \end{bmatrix} \tag{2}$$

where k_t is the motor torque constant.

The above model is different from the model commonly used for PM synchronous motors. When modeling a PM synchronous motor the d-axis is usually aligned with its rotor position [6]. However, since micro-stepping drives do not have positional sensor the frame axes can't be aligned with the rotor position correctly. Hence, a better model is to align the frame axes with the current vector. As shown in Eq. (1), depending on the magnitude and direction of the external load the rotor may be dragged behind or pushed ahead relative to the motor current vector.

III. Current Controller Design

A synchronous frame current regulator is proposed to facilitate micro-stepping control of the LSM. Figure 1 shows a block diagram of the control system. PI regulation is used for each axis, and the gains of both axes are set equal for convenience. A block diagram of the current controller is shown in Fig. 2. The blocks enclosed by dashed lines are the motor model. The current commands are denoted as i_{qe}^* and i_{de}^*. In general, i_{qe}^* is set to zero and i_{de}^* is set to the motor rated current. The third input, ω_e, is the excitation frequency. ω_e is determined from the required motor speed. The two trigonometric terms in Eq. (1), i.e. $\cos(\Delta\theta_e)$ and $\sin(\Delta\theta_e)$, are treated as disturbance inputs to the current controller since $\Delta\theta_e$ is a function of external load force.

Because the operating frequency of LSM is quite high, the roots of the current controller migrate considerably when the motor travels at speed. Therefore, as shown in Fig. 2, the terms containing ω_e in the motor model, i.e. $i_{qe}L\omega_e$ and $i_{de}L\omega_e$, are cancelled with two additional feedback loops. These voltages are calculated from the current feedbacks and summed with the output of the PI regulator. As a result, the roots that move with ω_e are removed from the characteristic equation, and the dynamic characteristics of the current controller do not change as ω_e varies.

Let $\hat{L}$ be the estimated winding inductance, the current responses can be expressed in terms of the command and the disturbance inputs as

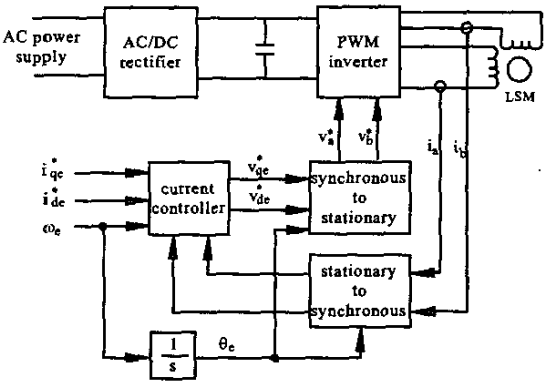

Fig. 1 Block diagram of the LSM control system

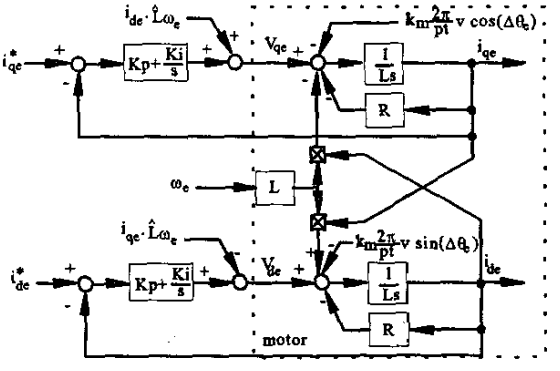

Fig. 2 Block diagram of the current controller

$$i_{qe} = \frac{Kp\cdot Ls^3 + (Kp\cdot r + Ki\cdot L + Kp^2)s^2 + (2Kp\cdot Ki + Ki\cdot r)s + Ki^2}{\Delta(s)} i_{qe}^* - \frac{\omega_e(L-\hat{L})(Kp\cdot s^2 + Ki\cdot s)}{\Delta(s)} i_{de}^* + \left(\frac{2\pi}{p_t}\right)\frac{v\omega_e k_m(L-\hat{L})s^2}{\Delta(s)}\sin(\Delta\theta_e) \tag{3}$$
$$-\left(\frac{2\pi}{p_t}\right)\frac{vk_m[Ls^3 + (r+Kp)s^2 + Ki\cdot s]}{\Delta(s)}\cos(\Delta\theta_e)$$

$$i_{de} = \frac{Kp\cdot Ls^3 + (Kp\cdot r + Ki\cdot L + Kp^2)s^2 + (2Kp\cdot Ki + Ki\cdot r)s + Ki^2}{\Delta(s)} i_{de}^* + \frac{\omega_e(L-\hat{L})(Kp\cdot s^2 + Ki\cdot s)}{\Delta(s)} i_{qe}^* - \left(\frac{2\pi}{p_t}\right)\frac{vk_m\omega_e(L-\hat{L})s^2}{\Delta(s)}\cos(\Delta\theta_e) \tag{4}$$
$$-\left(\frac{2\pi}{p_t}\right)\frac{vk_m[Ls^3 + (r+Kp)s^2 + Ki\cdot s]}{\Delta(s)}\sin(\Delta\theta_e)$$

where Kp and Ki are the proportional and the integral gain, respectively, of the current controller, and the characteristic equation is

$$\Delta(s) = L^2s^4 + 2L(Kp+r)s^3 + [(r+Kp)^2 + 2K_iL + (L-\hat{L})^2\omega_e^2]s^2 + 2K_i(r+K_p)s + Ki^2 \tag{5}$$

As shown in Eq.(5), $\Delta(s)$ is forth order because the q and the d axes are cross-coupled when the motor is controlled in the synchronous frame. However, as soon as the correct de-coupling voltages are summed to the controller, i.e. $\hat{L} = L$, the axes no longer cross-coupled and the system becomes a dual second order system with all poles independent to ω_e. Figure 3 compares the root loci of the current controller when ω_e varied from 0 to 1000 Hz without and with the voltage de-coupling. As can seen from this figure, the roots move noticeably if the coupling voltages are not cancelled. Equations (3) and (4) also indicate that the current response of both axes do not contain any steady state error for step input from either the command or the disturbance.

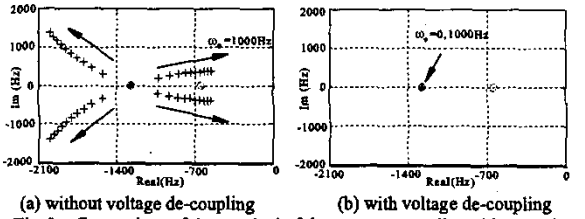

(a) without voltage de-coupling (b) with voltage de-coupling

Fig. 3 Comparison of the root loci of the current controller without and with the voltage de-coupling, ω_e varied from 0 to 1000 Hz

IV. PWM STRATEGY

Figure 4 shows a typical power circuit for two-phase LSM driven by three-phase voltage source inverter. The motor phase windings are connected in series. Each phase is connected to one inverter leg, and the common point between the two phases is connected to the third inverter leg. Comparing to traditional H-bridge circuits, this circuit has the advantages that it requires less power switches and can be used to drive either two-phase or three-phase motors. Nevertheless, PWM strategy for three-phase motor cannot be applied directly.

Let V_{qs} and V_{ds} be the stationary frame motor phase voltages, it can be seen from Fig. 4 that V_{qs} and V_{ds} are simply the differential voltages between a–c and b-c legs, and they can be expressed in matrix form as,

$$\begin{bmatrix} V_{ds} \\ V_{qs} \\ V_o \end{bmatrix} = \begin{bmatrix} 1 & 0 & -1 \\ 0 & 1 & -1 \\ 0 & 0 & 1 \end{bmatrix} \begin{bmatrix} V_a \\ V_b \\ V_c \end{bmatrix} \tag{6}$$

where V_a, V_b, and V_c are the inverter leg voltages, and V_o is the so-called 'zero sequence component' for the transformation to be unique [6]. Because the circuits seen by the inverter legs are imbalanced, V_a, V_b, and V_c do not have to sum to zero. In fact, V_o can be selected arbitrarily as long as it resides within the bus voltage V_i. In Eq. (6) V_c is set to V_o for convenience.

Each leg of a three-phase VSI can have two possible states: '1' where the upper switch is on, or '0' where the lower switch is on. Let the switching states for phase a, b, and c be S_a, S_b and S_c, respectively, the eight switching states and their corresponding leg and phase voltages are shown in Table 1. These 'space vectors' form an asymmetric hexagon in the dq plane, as shown in Fig. 5. Let V_{ds}^*, V_{qs}^* be the mean A-phase and B-phase reference voltages for the motor, then the reference voltages for inverter legs can be found by the inversion of Eq. (6) as,

$$\begin{bmatrix} V_a \\ V_b \\ V_c \end{bmatrix} = \begin{bmatrix} 1 & 0 & 1 \\ 0 & 1 & 1 \\ 0 & 0 & 1 \end{bmatrix} \begin{bmatrix} V_{ds}^* \\ V_{qs}^* \\ V_o \end{bmatrix} \tag{7}$$

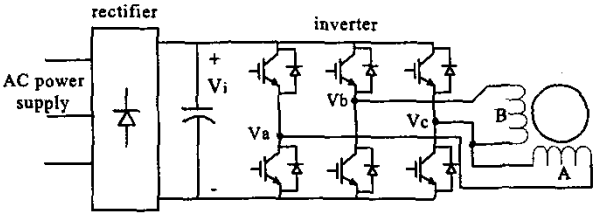

Fig. 4 Two-phase LSM driven by three-phase VSI

Table 1: Switching States, Inverter Voltages, and Phase Voltages

S_a	S_b	S_c	V_a	V_b	V_c	V_{ds}	V_{qs}
0	0	0	0	0	0	0	0
1	0	0	V_i	0	0	V_i	0
1	1	0	V_i	V_i	0	V_i	V_i
0	1	0	0	V_i	0	0	V_i
0	1	1	0	V_i	V_i	$-V_i$	0
0	0	1	0	0	V_i	$-V_i$	$-V_i$
1	0	1	V_i	0	V_i	0	$-V_i$
1	1	1	V_i	V_i	V_i	0	0

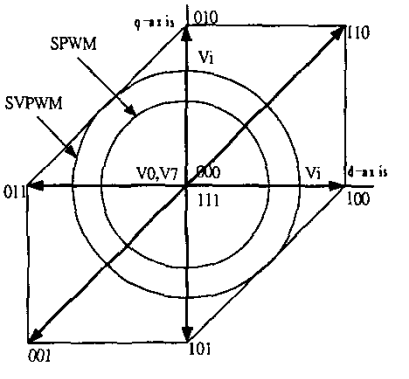

Fig. 5 Space vectors for two-phase motor driven by three-phase VSI

Equation (7) can be used to generate inverter leg voltages from motor reference phase voltages. Because the freedom of selecting V_o, this equation can be illustrated with a signal block diagram containing an injected voltage (V_o) calculator and a triangle-intersection based PWM as shown in Fig. 6. This diagram is very similar to the diagram for three-phase motor driven by three-phase VSI [7] except its input is consisted of two quadratic reference voltages and a zero.

It can be seen from Fig. 6 that if V_o is set to zero, i.e. $V_c = 0.5V_i$, then a conventional sinusoidal PWM (SPWM) is realized. This strategy is commonly employed in analog drives due to its simplicity in implementation. However, since V_c is fixed at $0.5V_i$ the maximum fundamental motor phase voltage attainable is only about half of the power supply without over-modulation. The inner circle shown in Fig. 5 indicates the voltage range for SPWM.

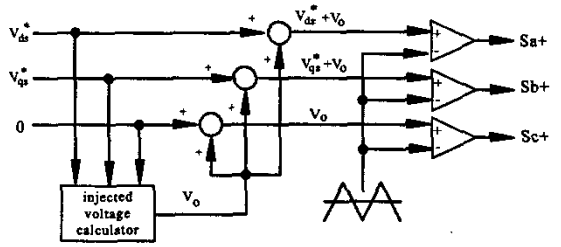

Fig. 6 Signal block diagram for a two-phase motor driven by three-phase PWM-VSI

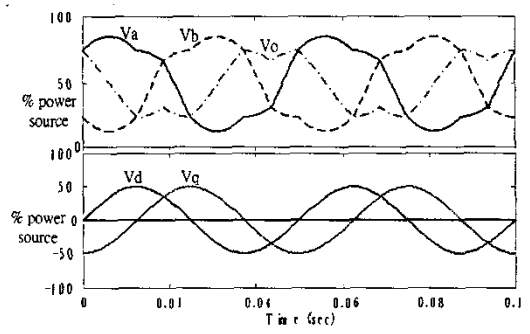

Fig. 7 Inverter leg voltages and motor phase voltages when the reference voltage is 50% of power source

V. Space Vector PWM

From the voltage-injection diagram shown in Fig 7 the space vector PWM commonly used for driving three-phase ac motors can be derived for two-phase motors. SVPWM is performed on the basis of the average voltage during one sampling period. A zero sequence signal is injected into all inverter leg voltages such that the zero voltage applying time is distributed symmetrically to the center of the sampling interval [7,8]. Based on this principle, two-phase SVPWM can be obtained by selecting V_o such that the non-zero voltage applying time is centered at the sampling interval. At any PWM control period, the maximum and the minimum applying voltage can be found as

$$V_{max} = \text{maximum } \{V_{ds}^*, V_{qs}^*, 0\}$$
$$V_{min} = \text{minimum } \{V_{ds}^*, V_{qs}^*, 0\} \quad (8)$$

Since the center of the non-zero voltage applying time is equivalent to the gating time for the average of V_{max} and V_{min}, the voltage required to bring the non-zero voltage applying time to the center of the sampling interval is

$$V_o = -(V_{max} + V_{min})/2 \quad (9)$$

Therefore, by selecting V_o as above the space vector PWM for two-phase motor is realized.

The outer circle shown in Fig. 5 indicates the voltage range attainable with the SVPWM. The maximum phase voltage with this scheme is approximately 70% of the power supply, which is about 20% more than SPWM. Figure 7 shows the simulated inverter leg and motor phase voltages for the SVPWM when the motor reference voltage is 50% of the input power source. It can be seen that V_a and V_b have significant harmonics due to the voltage injection but the motor phase voltages are sinusoidal. Also note that the sum of three inverter leg voltages is not zero.

VI. Dead-time Compensation

Because the loads seen by the inverter legs are not equal, motor currents will have different levels of magnitude and phase errors if the dead-time of the inverter power switches are not properly compensated. Many dead-time compensation techniques have been reported previously, for example [9]. In general, these techniques are all applicable to the drive system considered in this paper. The main difficulty of dead-time compensation is the prediction of zero-crossing instants of motor currents. But, as described in the previous sections, motor currents are regulated and their amplitude is controlled to a fixed value for micro-stepping drives. Therefore, zero-crossing instants can be predicted with reasonable accuracy if current following errors are small.

As presented in Section III, since the motor currents are regulated in the synchronous frame their following errors are very small when the motor is running at constant speed. Thus zero-crossing instants can be predicted simply with the angle of the reference current. Once an inverter leg current is detected to cross zero, a pre-measured voltage to correct the voltage error caused by dead-time is added to the leg voltages before they are converted to PWM signals. Note that this scheme does not need any adjustment for different reference speeds. It is a simple and effective dead-time compensation method for micro-stepping drives.

VII. Experimental Results

The proposed control scheme was implemented in a TMS320F2407 based DSP controller for experimental verifications. The experiments used a 110V, 3A, 1.8°, two-phase hybrid linear stepping motor, its parameters are shown in Appendix A. The sampling rate of the current controller is 10 Khz. At each sampling instant the current control, dead-time compensation, and space vector PWM are performed. Because the PWM always has one sampling period delay, the dead-time compensator was setup such that the compensating voltage was added to or subtracted from the voltage commands at the second sampling instant before the predicted current zero-crossing occurred. The dead-time of the power switches were about 3 μs.

Figure 8 shows the current responses in the stationary frame when the motor was running at 60, 300, and 600 mm/sec, respectively, the excitation frequencies corresponding to these speeds are 100, 500, and 1000 Hz, respectively. The amplitude of the commanding currents, i_{de}^* and i_{qe}^*, were set to 2 Amps and zero, respectively. As can be seen from this figure that the currents tracked their references quite well at all speeds. Although the shape of the motor current distorted slightly at high speeds, there were still in phase with each other.

To verify the space vector PWM technique presented in Section V, an experiment with the current controller disabled was performed. The voltage references were set to about 75 Volts and 100 Hz. Figure 9 shows the reference voltages and the measured fundamental voltages at the inverter legs. The shapes of the inverter leg voltages are very similar to the simulation results shown in Fig. 7.

Figure 10 compares the current responses when the dead-time of the power switches were (a) not compensated, and (b) compensated. The excitation frequency was 100 Hz. Figure 11 shows the current responses in vector forms. It can be seen that the waveforms shown in Figs. 10(a) and 11(a) have significant distortions due to the voltage errors caused by dead-time. On the contrary, as shown in Figs. 10(b) and 11(b), the waveforms became nearly sinusoidal when the dead-time was compensated for. These results shown that the proposed scheme can effectively compensate for the voltage errors due to dead-time.

VIII. Conclusions

This paper presented the theoretical analysis and experimental verifications of a control scheme for micro-stepping of two-phase linear stepping motor drives using three-phase voltage source inverters. The motor currents were controlled in the synchronous frame to reduce steady state error. The cross-coupling between motor phase currents were removed via additional feedback loops to preserve the dynamical characteristics of the current responses. A space vector PWM for the motor drive was also presented. The scheme is based on the principle of harmonic injection for three-phase motors. The maximum phase voltage attainable is about 70% of the source without over-modulation. The voltage errors due to dead-time were compensated for with a simple current zero-crossing detector. Good dynamic performances were obtained in the experimental verifications. The currents tracked their references closely at all speeds. The shape of the motor current distorted slightly at high speeds, but the phase error is very small.

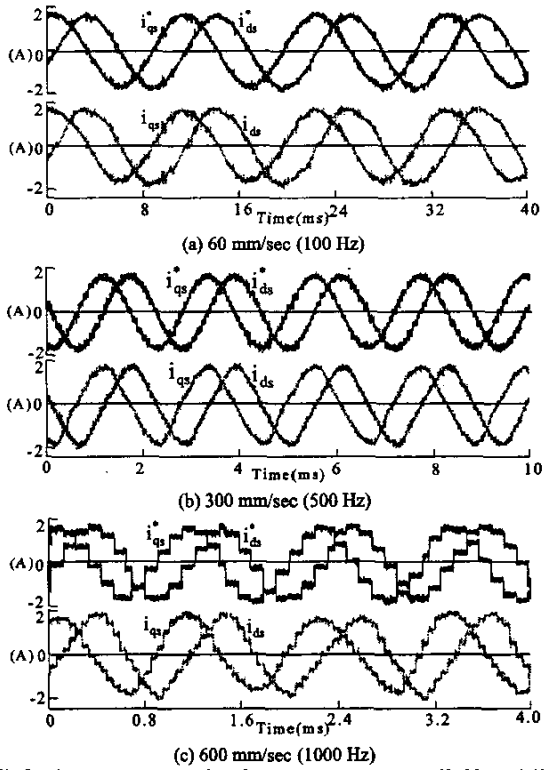

(a) 60 mm/sec (100 Hz)

(b) 300 mm/sec (500 Hz)

(c) 600 mm/sec (1000 Hz)

Fig.8 Current responses when the motor was running at 60, 300 and 600 mm/sec, respectively

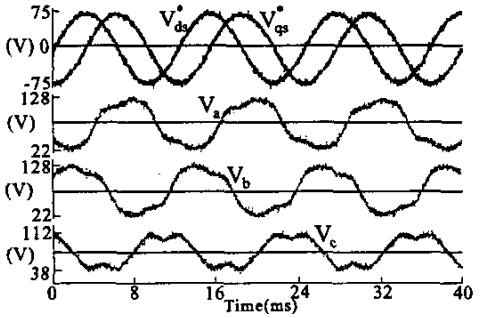

Fig. 9 Inverter leg voltages (fundamental) when the excitation voltages are sinusoidal signals and their frequency = 100Hz

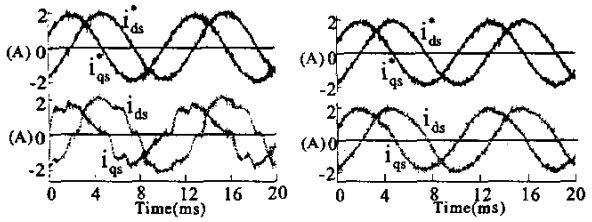

(a) without dead-time compensation (b) with dead-time compensation

Fig. 10 Comparison of current responses without and with dead-time compensation, excitation frequency = 100Hz

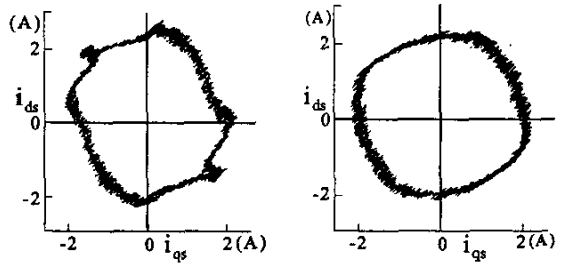

(a) without dead-time compensation (b) with dead-time compensation

Fig. 11 The current responses of Fig. 10 plotted as ids vs. iqs

APPENDIX A

The linear stepping motor used for the experimental verifications is a 110V, 3A, 1.8°, two-phase hybrid linear stepping motor. The motor parameters are:

Resistance (r)	8 Ω
Inductance (L)	15 mH
Stator pole number	40
Pole pitch	0.64 mm

ACKNOWLEDGMENT

We gratefully acknowledge the support for this research by the National Science Council, Taiwan, R. O. C., under grant: NSC 91-2213-E-032-033.

REFERENCES

[1] T. Kenjo and A. Sugawara, "*Stepping motors and their microprocessor controls*", Second Edition, Oxford University Press, 1994.

[2] P.W. Lee and C. Pollock, "Shared switch converter topology for a two phase bipolar drive hybrid stepping motor" 27th Annual IEEE-PESC '96 Conference Record, Vol. 1, 1996, pp. 127-133.

[3] M.A. Jabbar, A.M. Ambadkone, and Yanfeng, "DSP based space vector PWM drive for constant power operation of two-phase induction motors", IECON'01, Vol. 2, 2001, pp. 1166-1171.

[4] M.B. de R. Correa, C.B. Jacobina, A.M.N. Lima, and E.R.C. da Silva, "A three-leg voltage source inverter for two-phase ac motor drive system", IEEE Power Electronics Specialists Conference, Vol. 3, 2001 pp. 1458-1463.

[5] S.M. Yang and E.L. Kuo, "Damping control of two-phase hybrid stepping motors", *IEEE Transactions on Power Electronics*, Vol. 18, No. 3, May 2003.

[6] D.W. Novotny, and T.A. Lipo, "*Vector Control and Dynamics of AC Drives*", Oxford University Press, 1997.

[7] A.M. Hava, R.J. Kerkman, and T.A. Lipo, "Simple analytical and graphical methods for carrier-based PWM-VSI drives", *IEEE Transactions on Power Electronics*, Vol. 14, No. 1, Jan. 1999.

[8] D.W. Chung, S.K. Sul, and J.S. Kim, "Unified PWM technique for real time power conversion", Power Conversion Conference, Vol. 1, 1997, pp. 265-270.

[9] A.R. Munoz and T.A. Lipo, "On-line dead-time compensation technique for open-Loop PWM-VSI drives", *IEEE Transactions on Power Electronics*, Vol. 14, No. 4, Jul. 1999, pp.683-689.